ChemComm

COMMUNICATION

Check for updates

Graphdiyne aerogel architecture *via* a modified Hiyama coupling reaction for gas adsorption†

Qing Liu, Jiaqiang Li and Nikos Hadjichristidis [ID] *

Carbon aerogels are special porous materials with low density and large specific surface area and have advanced applications. As a new type of carbon nanomaterials, graphdiynes (GDY) aerogel possess a highly π-conjugated structure, unique sp/sp²-hybridized linkages, and well-distributed intrinsic pores, which endow GDY aerogel with great potential applications. However, the fabrication of macroscopic GDY aerogel is still an ongoing challenge due to intrinsic synthetic difficulties. Here, a modified Hiyama coupling reaction was developed to synthesize GDY aerogel *via* in-situ deprotection of trimethylsilane groups and subsequent freeze-drying. The synthesized GDY aerogel has a low density of $\sim$12 mg cm^{-3}, a high specific surface area of $\sim$909 m^2 g^{-1}, and a porosity of $\sim$98%, which is superior to other GDY nanomaterials. The adsorption capacity of GDY aerogel toward H_2, CO_2, and CH_4 is investigated, and competitive adsorption abilities are obtained.

Graphdiyne (GDY) is a new carbon allotrope that is composed of sp and sp² hybridized carbon atoms.[1] The highly π-conjugated structure, unique sp/sp²-hybridized linkages, and well-distributed intrinsic pores endow GDY with great potential applications for detector,[2] catalysis,[3] gas capture/separation,[4] and energy storage applications.[5] Since Li and co-workers first synthesized GDY in 2010,[6] tremendous efforts have been devoted to the preparation of GDY with different morphologies (*e.g.* GDY films,[7] nanowalls,[8] nanoribbons,[9] nanowires,[10] and nanosheets[2b,5b]) to fit better in abundant applications. GDY aerogel is considered as a new kind of carbon nanomaterial that features not only the unique properties of GDY, but also the distinctive merits of aerogels, leading to an attractive macroscopic 3D material with huge potential applications. However, the synthesis of GDY aerogel remains a significant challenge because of the intrinsic synthetic difficulties.

Physical Sciences and Engineering Division, King Abdullah University of Science and Technology (KAUST), Thuwal 23955, Saudi Arabia.
E-mail: nikolaos.hadjichristidis@kaust.edu.sa

† Electronic supplementary information (ESI) available. See DOI: https://doi.org/10.1039/d2cc05213j

Reviewing the reported synthetic methods of GDY nanomaterials, Glaser, Glaser–Hay, and Eglinton coupling of hexaethynylbenzene (HEB) are the mainly used methods to synthesize GDY nanomaterials, in which the instability of HEB is considered as one of the key problems affecting the formation of high quality GDY nanomaterials. Some researchers have demonstrated that the HEB turns brown rapidly in the presence of air and this phenomenon worsens as the monomer concentration increases.[11] However, for aerogel synthesis, relatively high monomer concentrations and long reaction time (several days) are required. Thus, using HEB as a monomer is difficult to synthesize GDY aerogel with high quality. Hexakis-[(trimethylsilyl)]ethynylbenzene (HEB-TMS), another monomer that can be used to synthesize GDY, exhibits higher stability than HEB in common organic solvents in air.[12]

Herein, we propose a feasible route for the preparation of GDY aerogel using HEB-TMS as a precursor *via* a three-step strategy. After evaluating copper salts and solvents, a modified Hiyama coupling reaction was employed to synthesize GDY aerogel using $Cu(OAc)_2$ as catalyst and pyridine as solvent, which is different from the traditional Hiyama coupling that uses CuI and polar solvents like *N,N*-dimethylformamide (DMF) or dimethyl sulfoxide (DMSO).[12] The modified Hiyama coupling system is a crucial modification that allows the coupling reaction to be carried out directly between HEB-TMS monomers with high conversion and polymerization under mild conditions. The combination of the high efficiency of the modified Hiyama coupling reaction and the free rotation of the alkyne–aryl and alkyne–alkyne single bonds leads to the formation of a 3D GDY aerogel. As a result, the obtained GDY aerogel exhibits low density, high specific surface area, and porosity. Compared with other porous organic materials, the GDY aerogel exhibits not only excellent gas adsorption capacity but also efficient recycling ability.

Fig. 1 illustrates the three-step synthetic route of GDY aerogel. First, a GDY organogel is obtained by modified Hiyama coupling. Then, the organogel undergoes a series of solvent exchanges to remove the side products and metal residues.
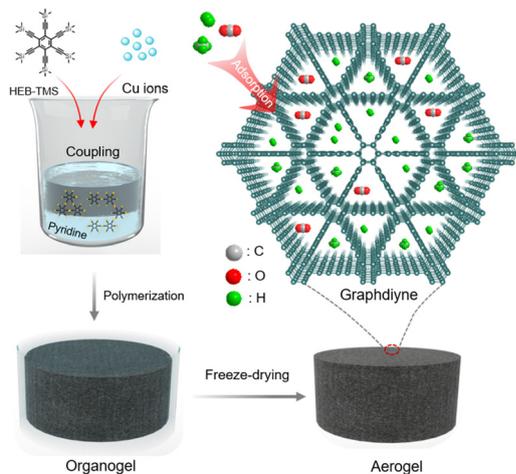
Fig. 1 Schematic illustration of the synthesis of monolithic GDY aerogels.

Finally, a monolithic GDY aerogel is formed after freeze-drying of the obtained organogel in water. In order to realize the modified Hiyama coupling reaction, two classic systems, Eglinton coupling and traditional Hiyama coupling, were investigated (Fig. S1, ESI†) and failed to form GDY aerogel monoliths (Fig. S1a–f, ESI†). To verify the efficiency and reliability of the modified Hiyama coupling system, a model reaction was performed under the same conditions to give the corresponding product of 1,3-diynes in over 99% yield (Fig. S2, ESI†). The conversion of HEB-TMS was also evaluated by nuclear magnetic resonance (NMR), with the conversion up to 99% (Fig. S3, ESI†).

After optimizing the reaction temperature, catalyst amount, and monomer concentration, the optimal GDY aerogel was obtained and used for subsequent characterization (Fig. S4 and S5, ESI†). Photographs with the synthetic details of the optimized conditions for the GDY aerogel are illustrated in

Fig. 2a, in which GDY aerogel has a low density (*ca.* 12 mg cm^{-3}) that can be easily supported by a few hairs of pennisetum. Scanning electron microscopy (SEM) images indicate that the aerogel exhibits a highly porous structure constructed by continuous and large-area networks (Fig. 2b and c). Transmission electron microscopy (TEM) images of the GDY aerogel further reveal that the networks are composed of highly wrinkled films (Fig. 2d and e). The high-resolution TEM (HRTEM) image shows that these wrinkled films have a layered structure with a lattice parameter of 0.365 nm, corresponding to the interlayer distance of GDY (Fig. 2f). A high-angle annular dark-field (HAADF) image and the corresponding energy-dispersive X-ray spectroscopy (EDS) element mapping images indicate that the carbon element is the dominant component with a homogeneous spatial distribution (Fig. 2g and Fig. S6, ESI†).

The quality and physical properties of the prepared GDY aerogel were carefully characterized. The Raman spectrum of GDY aerogel displays three dominant peaks that appeared at 1396, 1580, and 2179 cm^{-1} (Fig. 3a), which are consistent with the typical bands of GDY materials according to previously reported work.[5b] Compared to the Raman spectrum of HEB-TMS, the disappearance of the peak at 2156 cm^{-1} and the appearance of the peak at 2176 cm^{-1} in the GDY aerogel spectrum indicate the formation of conjugated diyne linkages.[6] The peaks at 1585 and 1395 cm^{-1} are ascribed to the G and D bands of GDY, respectively. It is worth noting that the peak at 1924 cm^{-1} representing a C_{sp}–Cu complex exhibits a weak intensity, indicating a relatively small portion of intermediate products in the GDY aerogel.[13] In the Fourier transform infrared (FT-IR) spectrum of the GDY aerogel, the bands at 1597 and 2103 cm^{-1} can be attributed to the skeletal vibration of the aromatic ring and the stretching vibration of C–C triple bonds, respectively.[6] The disappearance of the band of terminate alkynes at 2157 cm^{-1} indicates the high conversion of HEB-TMS. X-Ray photoelectron
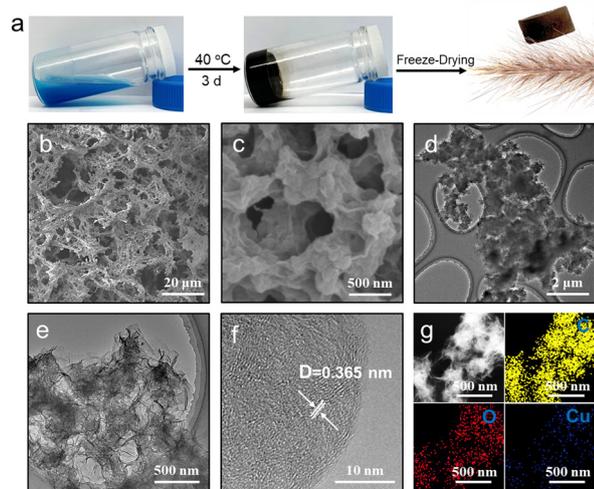
Fig. 2 (a) Photographs of the synthetic route of GDY aerogel. (b and c) SEM images and (d and e) TEM images of GDY aerogel obtained from freeze-drying. (f) HRTEM image of the GDY aerogel. (g) HAADF image and corresponding EDS mapping images of the GDY aerogel.
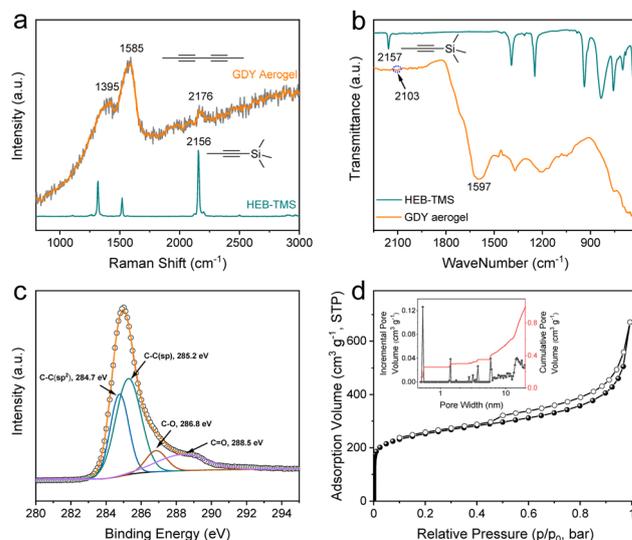
Fig. 3 (a) Raman and (b) FT-IR spectra of GDY aerogel and HEB-TMS. (c) XPS spectra of GDY aerogel for C 1s. (d) Nitrogen adsorption–desorption isotherms of the GDY aerogel. The inset is the pore size distribution curves.

spectroscopy (XPS) measurements indicate that the GDY aerogel is mainly composed of carbon element (Fig. S7, ESI†), which is consistent with the EDS results. The C 1s peak can be deconvoluted into four subpeaks at 284.7, 285.2, 286.8, and 288.5 eV, corresponding to C=C, C≡C, C–O, and C=O bonds, respectively (Fig. 3c). The existence of oxygen with medium intensity might result from the adsorption of air and some inevitable defects.[7c] The weak peaks of Cu and N might originate from the residual Cu-pyridine complex. There is an obvious bathochromic shift in the UV-vis spectra compared to the monomer of HEB-TMS (Fig. S8, ESI†), indicating that an extended π conjugated system is formed due to the increased polymerization degree of the monomers.[8a]

N$_2$ sorption analysis was conducted to probe the specific surface areas and porosity parameters of the GDY aerogels (Fig. 3d). The N$_2$ adsorption–desorption isotherms of the resultant aerogel feature a combination of type I and type IV isothermal profiles according to the IUPAC classification. A sharp uptake at low relative pressure was observed, indicating the presence of permanent micropores. In addition, the obvious hysteretic loop at the relatively high region indicates the presence of mesopores. The pore size distribution (PSD) following nonlocal density functional theory (NLDFT) further reveals that the GDY aerogel exhibits a dominant pore diameter of 0.538 nm that is close to the theoretical pore size of GDY (Fig. 3d inset).[4a] The Brunauer–Emmett–Teller (BET) surface area of the GDY aerogel was evaluated to be 909 m^2 g^{-1} (Fig. S9, ESI†), which is larger than most GDY nanomaterials and analogues reported elsewhere (Table S1, ESI†).[5a,14] As expected, the GDY aerogel with a macroscopic 3D structure and unique intrinsic microstructure has a porosity of *ca.* 98% (Fig. S10, ESI†), which is characteristic of typical aerogels (the porosity of aerogel samples is usually above 90%).[15]

Considering the high specific surface area, low density, and well-distributed intrinsic pores of GDY aerogel, it could be a promising material for gas storage or separation. With the nitrogen adsorption data of GDY aerogel in hand (Fig. S11, ESI†), we continued to investigate the adsorption capability of GDY aerogel for several gas molecules, including H$_2$, CO$_2$, and CH$_4$. As shown in Fig. 4a, H$_2$ (77 K), CO$_2$ (273 K) and CH$_4$ (273 K) are adsorbed up to 130.75 cm^3 g^{-1} (5.84 mmol g^{-1}), 87.31 cm^3 g^{-1} (3.89 mmol g^{-1}) and 26.12 cm^3 g^{-1} (1.16 mmol g^{-1}) at 1 bar, respectively. To compare with different porous materials, the CO$_2$ uptakes of other published materials at 273 K and 1 bar are summarized in Table S3 (ESI†), including covalent organic frameworks (COFs),[16] conjugated microporous polymers (CMPs),[17] hyper-cross-linked polymers (HCPs),[18] covalent triazine frameworks (CTFs),[19] porous aromatic frameworks (PAFs),[20] and porous organic cages.[21] The adsorption capacities of CO$_2$ are plotted in Fig. 4e as a function of BET specific surface area measured by N$_2$ adsorption at 77 K. These data indicate that the CO$_2$ uptake of GDY aerogel presents a competitive adsorption performance, which exceeds that of abundant porous organic materials, even those with much higher surface areas. On the other hand, the plot of CH$_4$ uptake *versus* BET specific surface area in Fig. 4f shows
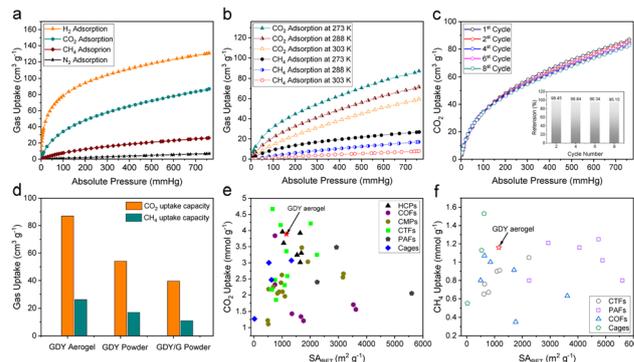
Fig. 4 (a) H$_2$ (77 K), CO$_2$ (273 K), CH$_4$ (273 K), and N$_2$ (273 K) adsorption isotherms of GDY aerogel. (b) CO$_2$ and CH$_4$ adsorption isotherms at 273, 288, and 303 K, respectively. (c) Cyclic performance of GDY aerogel for CO$_2$ adsorption. (d) Comparison of different GDY nanomaterials for CO$_2$ and CH$_4$ adsorption capacity at 273 K and 1 bar. (e) Plot of CO$_2$ uptakes measured at 273 K and 1 bar *vs.* BET specific surface area (SA$_{BET}$) calculated from N$_2$ adsorption at 77 K. (f) Plot of CH$_4$ uptakes measured at 273 K and 1 bar *vs.* SA$_{BET}$ calculated from N$_2$ adsorption at 77 K.

that the CH$_4$ uptake of GDY aerogel exceeds that of many CTFs (PCTF 1–7),[19b] and COFs (COF-10, COF-102, FECONF 1–2)[16,22] and is comparable to that of PAFs.[20] Besides, compared to the pristine GDY powder and the GDY/G heterostructure powder,[5c,6,14c] the CO$_2$ adsorption capacity of the GDY aerogel is 1.61 and 2.20 times higher, and the CH$_4$ adsorption capacity of the GDY aerogel is 1.54 and 2.38 times higher, respectively (Fig. 4d). Inspired by its good performance in gas adsorption at low pressure, we continued to investigate its gas capacity at extended pressures. GDY aerogel exhibits CO$_2$ uptake of 260 cm^3 g^{-1} (510 mg g^{-1}) at 10 bar (Fig. S12a–c, ESI†), which is even higher than that of COF-1, COF-6, and zeolites at 55 bar (220–350 mg g^{-1}).[16,23]

Selectivity is a crucial factor in evaluating the potential of a material for gas separation. From single-component adsorption isotherms, CO$_2$: N$_2$, CO$_2$: CH$_4$ and CH$_4$: N$_2$ selectivity values of up to 36 : 1, 9 : 1, and 8 : 1, respectively, are calculated from the simplified ideal adsorbed solution theory (IAST) model at a partial equilibrium pressure of 0.85 bar for N$_2$ and 0.15 bar for CO$_2$, 0.85 bar for CH$_4$ and 0.15 bar for CO$_2$, and 0.85 bar for N$_2$ and 0.15 bar for CH$_4$ in the bulk phase.[24] The GDY aerogel shows a selectivity of 36 for CO$_2$ over N$_2$, which is higher than that of poly(1,3,5-triethynylbenzene) (PTEB) aerogel (the selectivity is 25.9) with similar conjugated diacetylenic networks.[17c]

To further understand the adsorption properties of GDY aerogel toward CO$_2$ and CH$_4$, the isosteric heats of adsorption (Q_{st}) were calculated by the Clausius–Clapeyron equation. CO$_2$ and CH$_4$ adsorption isotherms were measured at 273, 288 and 303 K, respectively (Fig. 4b). For both gases, a higher temperature leads to lower gas uptake, indicating that the adsorption processes of GDY aerogel toward CO$_2$ and CH$_4$ are exothermic processes. The Q_{st} (CO$_2$) value of GDY aerogel was calculated to be 38 kJ mol^{-1} at low coverage (Fig. S13, ESI†), which explains the high adsorption of CO$_2$ at low pressure. Meanwhile, CH$_4$ adsorption isotherms for different temperatures provide an

unexpected Q_{st} value of 58 kJ mol^{-1} at low coverage (Fig. S14, ESI†).

Moreover, recycling materials has become more and more a part of our daily life. The recyclability of GDY aerogel can be tested simply by the adsorption–desorption process. As shown in Fig. 4c, after 8 adsorption–desorption cycles, the aerogel can maintain over 95% adsorption capacity for CO_2 even without reactivating the aerogel, thus indicating the excellent cyclability of GDY aerogel for gas storage. Considering its good cyclability, highly porous structure, and free-standing 3D monoliths, the GDY aerogel should be a promising absorbent for organic solvents. The aerogel possesses absorption capacity for different solvents ranging from 22–40 times its own weight (Fig. S15, ESI†), which is comparable to graphene aerogel and poly(vinyl alcohol)/carbon nanotubes (PVA/CNTs) aerogel, and higher than that of homocoupled conjugated microporous polymer (HCMP) networks (Table S2, ESI†).[25]

In summary, a modified Hiyama coupling reaction was developed to synthesize GDY aerogel monoliths, where HEB-TMS, Cu(OAc)$_2$, and pyridine were used as the precursor, catalyst, and solvent, respectively. Coupling of HEB-TMS directly without pre-deprotecting the TMS groups efficiently avoids the decomposition of terminal alkyne groups in the long reaction period. The synthesized GDY aerogel exhibits low density (*ca.* 12 mg cm^{-3}), high specific surface area (*ca.* 909 m^2 g^{-1}), and porosity (*ca.* 98%). The GDY aerogel also possesses impressive gas uptakes toward H_2, CO_2, and CH_4 from 1 bar to 10 bar, which are competitive with those of GDY-based nanomaterials and many porous organic materials. This work not only expands the applications of GDY but also provides a new synthetic strategy for GDY nanomaterials.

Conflicts of interest

There are no conflicts to declare.

Notes and references

1 (*a*) M. M. Haley, S. C. Brand and J. J. Pak, *Angew. Chem., Int. Ed. Engl.*, 1997, **36**, 836; (*b*) Y. Li, L. Xu, H. Liu and Y. Li, *Chem. Soc. Rev.*, 2014, **43**, 2572; (*c*) C. Huang, Y. Li, N. Wang, H. Liu and Y. Li, *Chem. Rev.*, 2018, **118**, 7744; (*d*) F. Fang, Y. Liu, L. Qi, Y. Xue and Y. Li, *Chem. Soc. Rev.*, 2022, **51**, 2681; (*e*) F. He and Y. Li, *CCS Chem.*, 2022, **5**, 72.

2 (*a*) N. Parvin, Q. Jin, Y. Wei, R. Yu, B. Zheng, L. Huang, Y. Zhang, L. Wang, H. Zhang, M. Gao, H. Zhao, W. Hu, Y. Li and D. Wang, *Adv. Mater.*, 2017, **29**, 1606755; (*b*) C. Wang, P. Yu, S. Guo, L. Mao, H. Liu and Y. Li, *Chem. Commun.*, 2016, **52**, 5629; (*c*) Z. Jin, Q. Zhou, H. Liu, J. Wang and Y. Li, *Adv. Mater.*, 2016, **28**, 3697.

3 (*a*) H. Qi, P. Yu, Y. Li and L. Mao, *J. Am. Chem. Soc.*, 2015, **137**, 5260; (*b*) Y. Xue, H. Liu and Y. Li, *Nat. Commun.*, 2018, **9**, 1460; (*c*) H. Yu, Y. Xue, B. Huang and Y. Li, *Natl. Sci. Rev.*, 2021, **8**, nwaa213; (*d*) L. Hui, F. He and Y. Li, *J. Am. Chem. Soc.*, 2022, **144**, 1921; (*e*) Y. Gao, Y. Xue, F. He and Y. Li, *Nat. Commun.*, 2022, **13**, 5227; (*f*) Y. Gao, Y. Xue, F. He and Y. Li, *PANS*, 2022, **119**, e2206946119; (*g*) X. Zheng, Y. Xue, C. Zhang and Y. Li, *CCS Chem.*, 2022, DOI: **10.31635/ccschem.022.202202189**.

4 (*a*) H. Zhang, X. He, M. Zhao, M. Zhang, L. Zhao, X. Feng and Y. Luo, *J. Phys. Chem. C*, 2012, **116**, 16634; (*b*) M. Bartolomei, E. Carmona-Novillo, M. I. Hernández, J. Campos-Martínez, F. Pirani and G. Giorgi, *J. Phys. Chem. C*, 2014, **118**, 29966.

5 (*a*) J. Li, J. Xu, C. Chen, J. Zhang and Z. Liu, *Adv. Mater.*, 2018, **30**, 1800548; (*b*) H. Shang, Z. Zuo, L. Li, F. Wang, H. Liu, Y. Li and Y. Li, *Angew. Chem., Int. Ed.*, 2018, **57**, 774; (*c*) J. Li, Y. Yi, X. Zuo, L. Tong, R. Shao, J. Sun and J. Zhang, *ACS Nano*, 2022, **16**, 3163.

6 G. Li, Y. Li, H. Liu, Y. Guo, Y. Li and D. Zhu, *Chem. Commun.*, 2010, **46**, 3256.

7 (*a*) R. Matsuoka, R. Sakamoto, K. Hoshiko, S. Sasaki, H. Masunaga, K. Nagashio and H. Nishihara, *J. Am. Chem. Soc.*, 2017, **139**, 3145; (*b*) C. Yin, J. Li, H. Peng, L. Tong and J. Zhang, *Adv. Funct. Mater.*, 2020, **30**, 2001396; (*c*) H. Yan, P. Yu, G. Han, Q. Zhang, Y. Li and L. Mao, *Angew. Chem., Int. Ed.*, 2019, **58**, 746; (*d*) J. Li, Y. Xiong, Z. Liu and J. Zhang, *ACS Appl. Mater. Interfaces*, 2019, **11**, 2734.

8 J. Zhou, X. Gao, R. Liu, Z. Xie, G. Zhang, H. Liu, Y. Li, J. Zhang and Z. Liu, *J. Am. Chem. Soc.*, 2015, **137**, 7596.

9 Z. Jia, Y. Li, Z. Zuo, H. Liu, D. Li and Y. Li, *Adv. Electron. Mater.*, 2017, **3**, 1700133.

10 X. Qian, Z. Ning, Y. Li, H. Liu, Q. Chen and Y. Li, *Dalton Trans.*, 2012, **41**, 730.

11 R. Diercks, J. C. Armstrong, R. Boese and K. P. C. Vollhardt, *Angew. Chem., Int. Ed. Engl.*, 1986, **25**, 268.

12 K. Ikegashira, Y. Nishihara, K. Hirabayashi, A. Mori and T. Hiyama, *Chem. Commun.*, 1997, 1039.

13 J. Li, Z. Zhang, Y. Kong, B. Yao, C. Yin, L. Tong, X. Chen, T. Lu and J. Zhang, *Chemistry*, 2021, **7**, 1284.

14 (*a*) Z. Zuo, H. Shang, Y. Li and Y. Li, *Chem. Commun.*, 2017, **53**, 8074; (*b*) J. He, N. Wang, Z. Yang, X. Shen, Y. Yi, Z. Tu and Y. Li, *Nat. Commun.*, 2017, **8**, 1172; (*c*) J. Li, L. Zhong, L. Tong, Y. Yu, Q. Liu, S. Zhang, C. Yin, L. Qiao, S. Li, R. Si and J. Zhang, *Adv. Funct. Mater.*, 2019, **29**, 1905423; (*d*) Y. Zhao, N. Yang, S. Li, L. Gu, K. Lin and D. Wang, *J. Am. Chem. Soc.*, 2019, **141**, 7240.

15 A. C. Pierre and G. M. Pajonk, *Chem. Rev.*, 2002, **102**, 4243.

16 H. Furukawa and O. M. Yaghi, *J. Am. Chem. Soc.*, 2009, **131**, 8875.

17 (*a*) J. R. Holst, E. Stöckel, D. J. Adams and A. I. Cooper, *Macromolecules*, 2010, **43**, 8531; (*b*) S. Ren, R. Dawson, A. Laybourn, J. X. Jiang, Y. Khimyak, D. J. Adams and A. I. Cooper, *Polym. Chem.*, 2012, **3**, 928; (*c*) R. Du, N. Zhang, H. Xu, Q. Zhao, Z. Liu and J. Zhang, *Adv. Mater.*, 2014, **26**, 8053.

18 (*a*) B. Li, R. Gong, C. Hu and B. Tan, *Macromolecules*, 2011, **44**, 2410; (*b*) C. F. Martín, E. Stöckel, R. Clowes, D. J. Adams, A. I. Cooper, J. J. Pis, F. Rubiera and C. Pevida, *J. Mater. Chem.*, 2011, **21**, 5475; (*c*) R. Dawson, L. A. Stevens, M. W. Smith, D. J. Adams and A. I. Cooper, *J. Am. Chem. Soc.*, 2012, **134**, 10741.

19 (*a*) S. Ren, M. J. Bojdys, R. Dawson, A. Laybourn, Y. Z. Khimyak, D. J. Adams and A. I. Cooper, *Adv. Mater.*, 2012, **24**, 2357; (*b*) Y. Zhao, K. X. Yao, B. Teng, T. Zhang and Y. Han, *Energy Environ. Sci.*, 2013, **6**, 3684.

20 T. Ben, C. Pei, D. Zhang, J. Xu, F. Deng, X. Jing and S. Qiu, *Energy Environ. Sci.*, 2011, **4**, 3991.

21 (*a*) T. Tozawa, J. T. Jones, A. Trewin, J. Bacsa, A. M. Slawin, A. Steiner and A. I. Cooper, *Nat. Mater.*, 2009, **8**, 973; (*b*) J. T. Jones, T. Hasell, X. Wu, J. Bacsa, F. Cora, B. Slater, A. Steiner, G. M. Day and A. I. Cooper, *Nature*, 2011, **474**, 367.

22 P. Mohanty, L. D. Kull and K. Landskron, *Nat. Commun.*, 2011, **2**, 401.

23 S. Cavenati, C. A. Grande and A. E. Rodrigues, *J. Chem. Eng. Data*, 2004, **49**, 1095.

24 (*a*) W. Lu, J. P. Sculley, D. Yuan, R. Krishna, Z. Wei and H. C. Zhou, *Angew. Chem., Int. Ed.*, 2012, **51**, 7480; (*b*) C. Xu and N. Hedin, *J. Mater. Chem. A*, 2013, **1**, 3406.

25 (*a*) J. Wang, Z. Shi, J. Yin and G. Hu, *J. Mater. Chem.*, 2012, **22**, 22459; (*b*) D. Tan, W. Fan, W. Deng and C. Meng, *Eur. Polym. J.*, 2012, **48**, 705; (*c*) C. B. Ma, B. Du and E. Wang, *Adv. Funct. Mater.*, 2017, **27**, 1604423.